Absolute Emission from the Mid-infrared to the Extreme Ultraviolet from a Pulsed Plasma Thruster (PPT)

IEPC-2007-268

Presented at the 30th International Electric Propulsion Conference, Florence, Italy
September 17-20, 2007

Edward J. Beiting [*], Jun Qian [†], Ray W. Russell[‡] and James E. Pollard[§]
The Aerospace Corporation, Los Angeles, CA 90009

Will Caven[**] and Ron Corey[††]
Space Systems/Loral, Palo Alto, CA 94303

Emission from the mid infrared to the extreme ultraviolet from a solid Teflon® pulsed plasma thruster (PPT) was observed. The PPT discharged with an electric energy of 40 Joules/pulse of at a pulse rate of 1 Hz. Absolute emission from most of the 1 nm to 15,000 nm segment of the electromagnetic spectrum was measured. This was accomplished using three instruments. A double prism spectrograph equipped with helium-cooled array detectors recorded emission from 2000 nm to 13,500 nm; data in 6000-8000 nm was discarded due to technical issues. A mid-range near IR-UV instrument recorded emission from 200 -1000 nm with 1 nm resolution. Finally, a 10 channel photometer registered emission from 1 – 190 nm. Significant emission was observed by all instruments and most discrete emissions have been identified as originating from carbon and fluorine and their ions.

Nomenclature

A	=	amplitude of oscillation
a	=	cylinder diameter
C_p	=	pressure coefficient
Cx	=	force coefficient in the x direction
Cy	=	force coefficient in the y direction
c	=	chord
dt	=	time step
Fx	=	X component of the resultant pressure force acting on the vehicle
Fy	=	Y component of the resultant pressure force acting on the vehicle
f, g	=	generic functions
h	=	height
i	=	time index during navigation
j	=	waypoint index
K	=	trailing-edge (TE) nondimensional angular deflection rate

[*] Senior Scientist, The Aerospace Corporation, edward.j.beiting@aero.org.
[† †] Research Scientist, The Aerospace Corporation, jun.qian@aero.org.
[‡ ‡] Senior Scientist, The Aerospace Corporation, ray.russell@aero.org.
[§ §] Senior Scientist, The Aerospace Corporation, james.e.pollard@aero.org.
[**] Spacecraft Payload Systems Engineer, Space Systems/Loral, caven.will@ssd.loral.com.
[††] Spacecraft Propulsion Subsystems Engineer, Space Systems/Loral, corey.ron@ssd.loral.com.

I. Introduction

A solid Teflon® pulsed plasma thruster (PPT) manufactured by Aerojet was tested at The Aerospace Corporation under a contract with Space Systems/Loral, the purpose of which was to determine compatibility of PPTs with various spacecraft payloads. The objectives were to characterize the PPT with respect to spacecraft contamination potential, electromagnetic compatibility, and plume emission at wavelengths from the soft x-ray to the mid-infrared. Space Systems/Loral provided the Modular Test Unit PPT[1], a set of drive electronics, and the wiring harness. Aerospace provided the vacuum chamber, all test instrumentation, facility data systems, and was responsible for the data reduction presented here. This paper describes the wavelength-resolved plume emission studies from the mid-infrared to the soft x-ray segment of the electromagnetic spectrum. Electromagnetic emission from DC to 17 GHz is presented in another paper at this conference [2].

This paper is organized in six sections. After the facility configuration is described in section II, the mid infrared measurements are presented in Section III, the visible-ultraviolet results in Section IV, and the vacuum ultraviolet – soft x-ray data in Section V. A discussion of the results is given in section VI.

II. Facility Configurations and Test Sequence

The thruster was operated in a 2.4-m diameter × 9.8-m long cryopumped vacuum chamber. Carbon composite sheets and flexible graphite lined the beam dump region of the chamber to minimize the yield of sputtered material. Two re-entrant cryopumps were on the end-dome behind the thruster, two more re-entrant pumps were in the beam dump region, and three 1.3-m cryotubs were mounted on the cylindrical wall of the tank adjacent to the thruster. To reduce liquid nitrogen consumption, a subset of 3 to 5 pumps was operated during the most of the plume tests, which gave a time constant for chamber pump-down of about 500 ms.

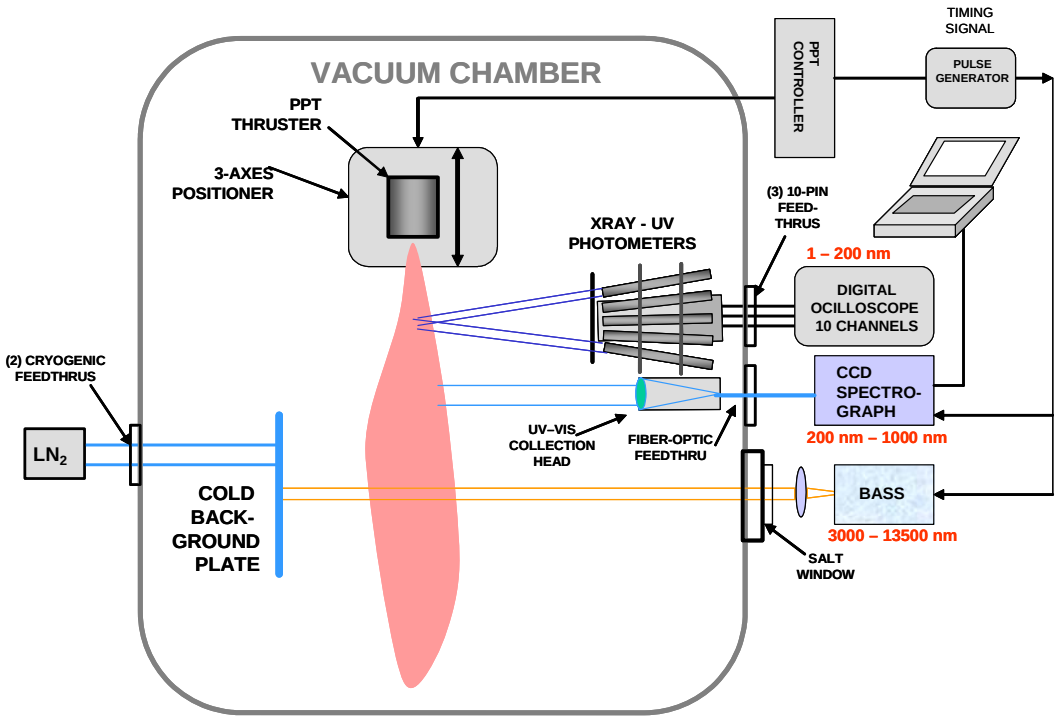

The principal components of the PPT were the anode plate, cathode plate, discharge initiator (spark plug), Teflon® propellant bar, rectangular exhaust nozzle, energy storage capacitor, high voltage transformer, and drive circuits. The propellant bar was fed through the back of the thruster body by a spring. A wiring harness and vacuum feed-through connected the PPT to a 28-VDC, 5-A power supply and to a trigger generator that commanded the firing of the spark plug and main capacitor.

Chamber background pressure was measured with an ionization gauge (Granville-Phillips 360) mounted to a flange on the chamber wall 1.4 m from the PPT. Base pressure with the thruster off was 1.5×10^{-7} torr after 30 hours

of pumping, with 90% of the residual gas being water vapor, and the remainder being air and hydrocarbons. A facility data acquisition system recorded the background pressure and thruster temperature throughout the test and provided a pressure interlock for the PPT power supply. When firing the PPT at 1 Hz with a discharge energy of 40 J, the time-averaged pressure rise was $\Delta P_{avg} = 1.5\times10^{-7}$ torr, as governed by the chamber pumping speed. Peak pressure rise at 25 ms after the firing event was $\Delta P_{pk} = 4.5\times10^{-7}$ torr, as governed by the ejected propellant mass and by the chamber volume. Weighing the propellant bar before and after a period of mostly nominal firing at 1 Hz (1 Aug to 4 Aug 2005) gave a mass change of 18.02 g in 275,960 pulses, corresponding to an ejected mass of 65.3 μg/pulse.

With the PPT positioned in the main chamber such that its plume impinges on the west wall beam dump, all the optical instruments were placed along the south side of the chamber as shown in Figure 1. The thruster was mounted on a 3-axis positioner that allowed any point in the plume to be studied up to a distance of 1 meter from the thruster exit. The mid-infrared instrument was located completely outside the chamber, viewing the plume through a salt (NaCl) window. The UV-IR instrument was also located outside the chamber but an interior optical head collected the radiation and transmitted it through the vacuum wall to the instrumentation via an optical fiber. The 10-barrel photometer used for the soft x-ray/uv measurements was located completely inside the vacuum chamber, passing only electrical signals to the recording electronics. The measurements were taken on different days: mid-IR first, followed by the x-ray/UV data, and finally the mid-range UV-IR spectrograph. Data acquisition by these instruments was triggered using a timing signal derived from a firing pulse from the PPT controller.

III. Mid Infrared Emissions

The Broadband Array Spectrograph System (BASS) Sensor is a helium-cooled dual prism, dual linear BIBIB Si:As array with each channel equipped with a transimpedance amplifier.[3] It has two 58-element detectors that are sampled at a rate of 200 Hz yielding a time resolution of 5 ms. It is generally used with a telescope but in this application an off-axis parabola mounted with its focus at the entrance field stop collected light in a ~2 cm diameter collimated beam. This beam viewed the plume through a NaCl window against a LN_2 cooled cold plate (see Fig. 1). The cold plate presented a low IR intensity background field, increasing the sensitivity of the instrument. The instrument and cold plate are pictured in Fig. 2. A dry nitrogen purge was used inside a plastic housing to minimize atmospheric transmission effects in the 1.2 m separation between the Dewar window on the BASS instrument and the chamber port.

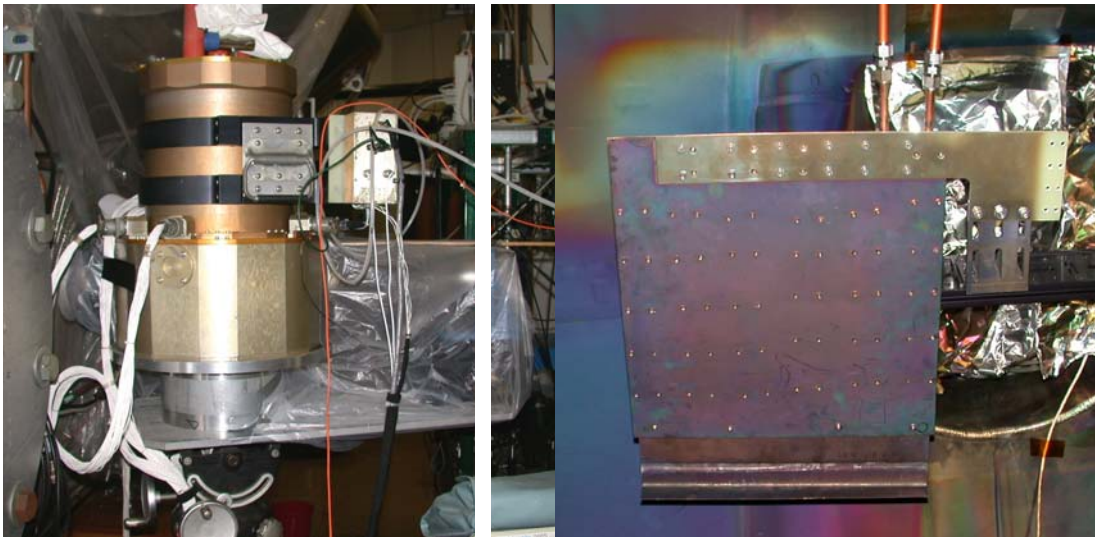

Figure 2. BASS instrument outside chamber (left); LN2 cold back plate inside chamber (right).

Each detector had both DC and AC electrical outputs. The AC was designed to respond to transient signals and had a gain of 40; the DC output operated at unity gain. The system has low-pass 80 Hz filters on the outputs and sampled the whole spectrum (116 channels) every 5 ms. A visible sensor output connected to one "data channel" was used to indicate which of the 5 ms samples contained the data.

The DC response of the BASS instrument was calibrated using a blackbody operating a 40 C and 70C.* Calibration uncertainty resulted from: temperature, emissivity uncertainty of calibration of the blackbody (1-5%); emission falling within the sample interval, uncertainty in the location of the collimated beam in the thruster exit stream, and the lack of repeatability of the thruster pulses (20%); and observed lack of file-to-file repeatability after averaging many samples (3-5%). Wavelengths were calibrated using a grating monochromator and a 5th and 4th order polynomial fits for short and long wavelength segments, respectively. Residuals were comparable to monochromator setting errors of 0.003 μm. The wavelength uncertainty should be considered on the order of the channel intervals which vary between 0.01 μm and 0.1 μm.

Between 1900 and 2000 spectral samples/file used for each "signal" spectrum for the data taken near the exit plane and 50 cm downstream of the exit plane. Approximately 900/file were collected for the data taken 100 cm from the exit plane. About 190 times as many additional spectra (samples) without the trigger pulse present were used to provide the average background to subtract from the data with the trigger pulse. Subtracting the average (non-pulse containing) samples from the average of the pulse-containing spectral samples and applying the calibrations yielded the final spectra. Data have been reduced and calibrated in absolute units, although optical depth and fill factor are unknown. Two sets of measurements were taken to assess repeatability at each distance from the thruster nozzle.

Figures 3 – 5 show the emission spectra from the plume at the exit plane, 50 cm, and 100 cm downstream of the exit plane, respectively. The 6 – 8 μm gap in these spectra was necessitated by significant absorption by the R and P branches of water, degradation of the data by a reflection-to-transmission transition near 6.5 um, and by occasional under-sampling of the arrays in this overlap region of the two arrays. Each figure displays two spectra, each from data runs taken at different times, illustrating the reproducibility of the data. The exit plane data in Figure 3.3 show emission peaks at 2.70-2.81 μm, 3.67-3.75 μm, 4.42 μm, 8.13 μm, and elevated region from 8-9 μm. Identical emission is seen in the data acquired 100 cm down stream from the exit plane but at about a third of the intensity. At the 50 cm position emissions are seen at 2.59-2.70 μm, 3.67-3.75 μm, 4.42 μm, and elevated region from ~8 – 9 μm at intensities at about 10 – 25 % that seen at the exit position, *i.e.*, the intensity is greater at the 100 cm position than at the 50 cm position.

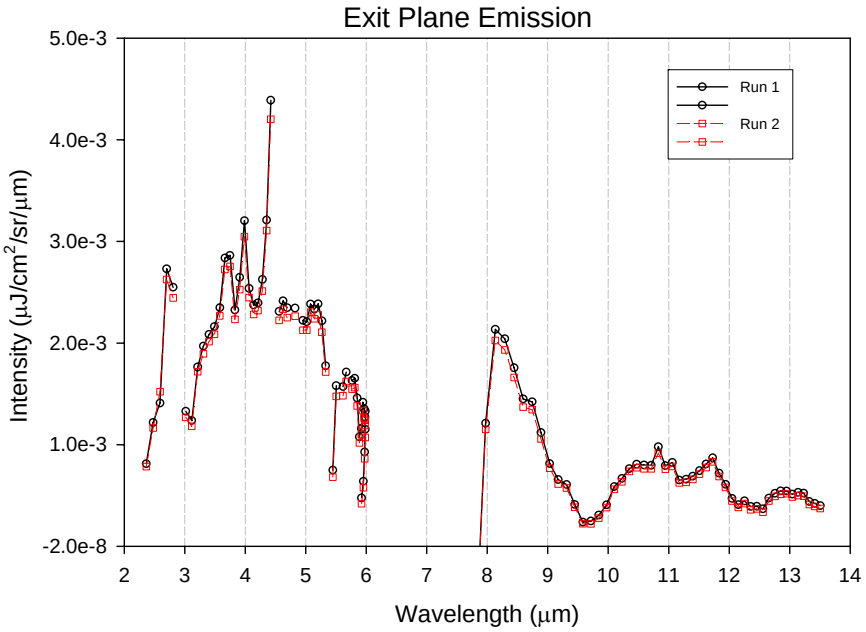

Figure 3. Spectra at exit plane.

*The blackbody was calibrated using a commercial camera and shown to be within ~1C of set point, with emissivity of 0.98 and with <1C gradient across it. The DC responsivity of the sensor = [Planck(70C) – Planck(40C)] / [(Signal(70C) – Signal(40C)]. The AC responsivity was the gain factor of 40X less.

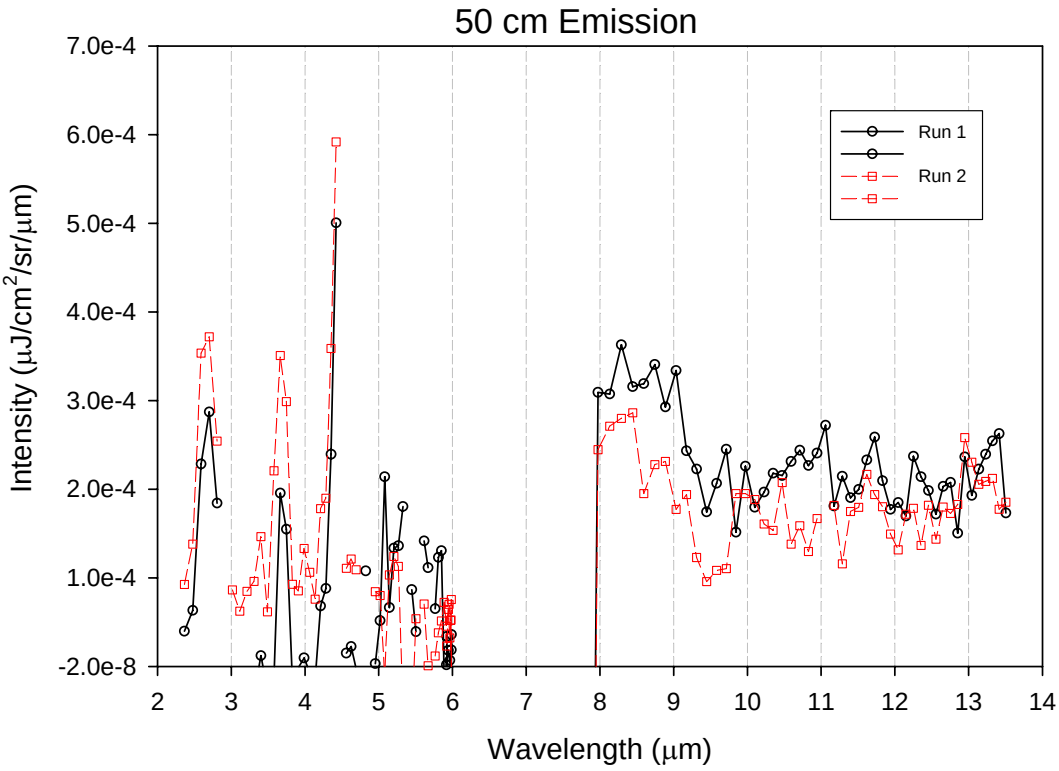

Figure 4. Spectra at 50 cm downstream of exit plane.

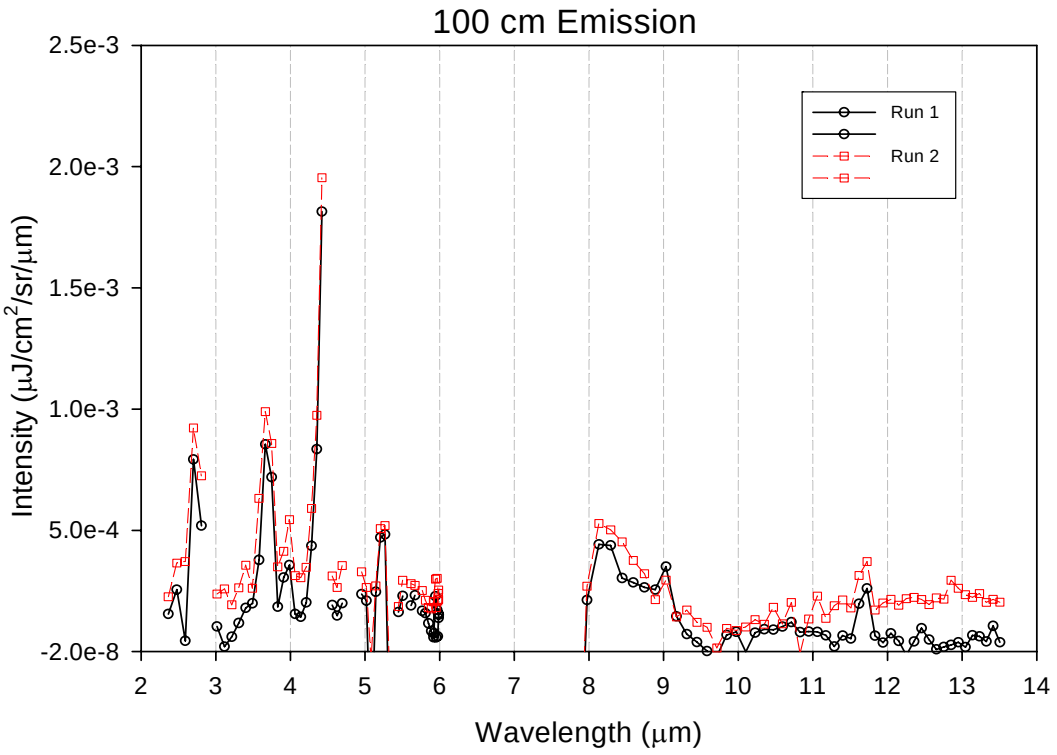

Figure 5. Spectra 100 cm downstream of exit plane.

IV. Near Infrared–Ultraviolet Spectra

An instrument was assembled to capture emission for the PPT from 200 – 1000 nm in a single spectral segment. This instrument used an Ocean Optics HR4000 spectrograph equipment with a 25 µm wide entrance slit, a 300 l/mm grating and a 3648 element CCD detector. This combination yields a spectral resolution of approximately 1 nm. Emission from the PPT plume was collected with an objective that was corrected for chromatic aberration across the entire 200 – 1000 nm range of the spectrograph. The RMS focal spot size of this triplet lens is 49 µm. This small spot size leads to efficient coupling to the 100-µm diameter optical fiber. The 0.12 numerical aperture of the fiber is equivalent to an F/4.2 optical system, assuring efficient coupling to the F/4 spectrograph. The 100-µm diameter fiber passed 32% of its exiting light through the 25 µm wide x 1 mm high slit. A diagram of the configuration is shown in Fig. 6.

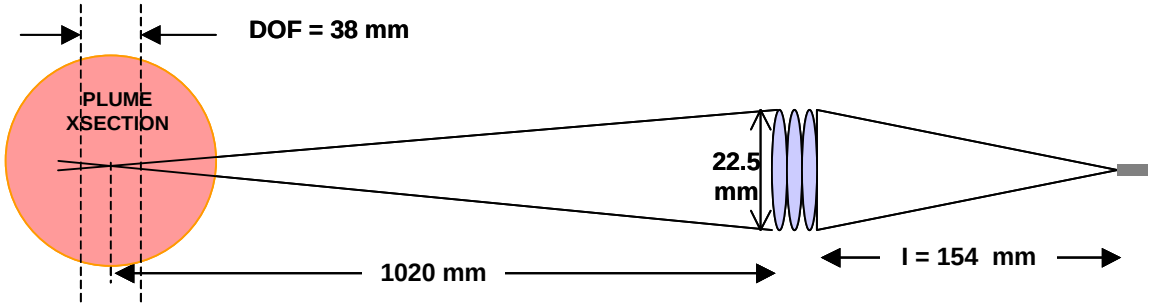

Figure 6. Collection geometry used to collect the near IR-UV spectra.

The positioning of the elements inside the vacuum chamber is show in Figure 1. The objective lens was located 1.02 m from the plume requiring a lens-fiber distance of 154 mm. The combination of aperture size and fiber diameter yields a depth-of-field of 38 mm. The absolute intensity calibration of the instrument was accomplished using a deuterium lamp for 200 - 400 nm spectral interval and a tungsten lamp in the 450 – 1000 nm interval. The calibration values for the 400 –550 nm interval were obtained by interpolation.

Measurements were at six positions along the centerline of thruster plume. A seventh measurement was made at the empirically determined position of maximum emission which was slightly off centerline near the exit plane. The positions of the measurements are shown in Figure 7.

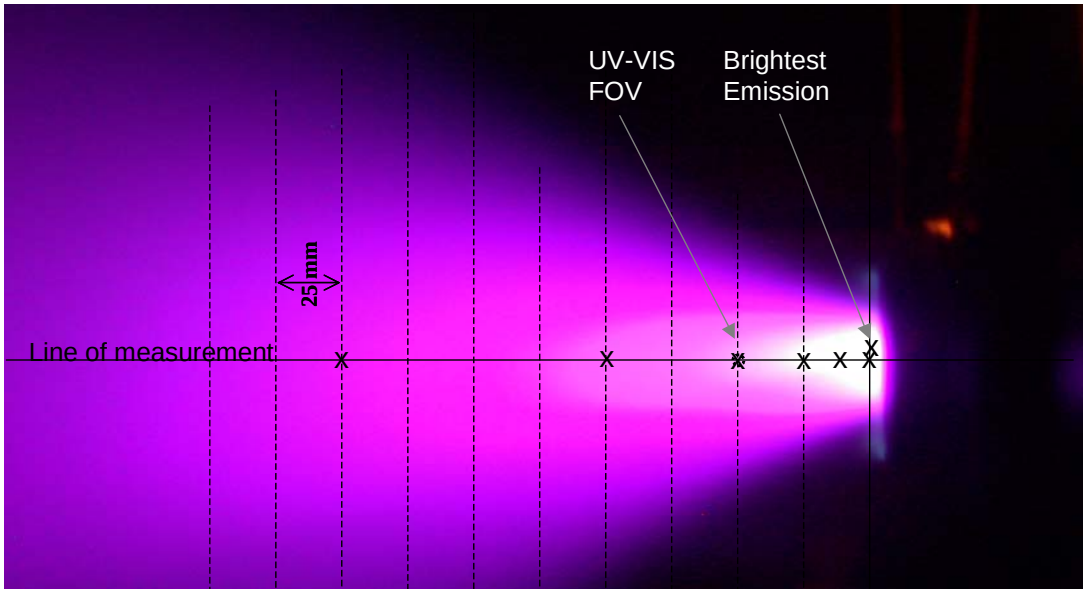

Figure 7. Measurement locations for the IR-UV instrument.

The maximum intensity spectrum is presented in two segments in Figures 8 and 9. Approximately 75 spectral features (atomic and ionic lines, molecular bands) could be discerned in this spectrum. Fifty-one (51) of these features can be assigned to F, F^+, C^+, and C^{2+}, the chemical constituents of Teflon® $(CF_2)_n$. Some of these emissions from a PPT have been identified in the 350 -750 nm spectra reported previously.[4] Greatest intensity is near the exit plane; here a maximum intensity of 100 μJ/pulse/cm^2/sr/nm for a line of F^+ at 385 nm was registered. The spectra as a function of position are shown in Figure 10. Spectral irradiance decreases monotonically a function of distance from the exit plane.

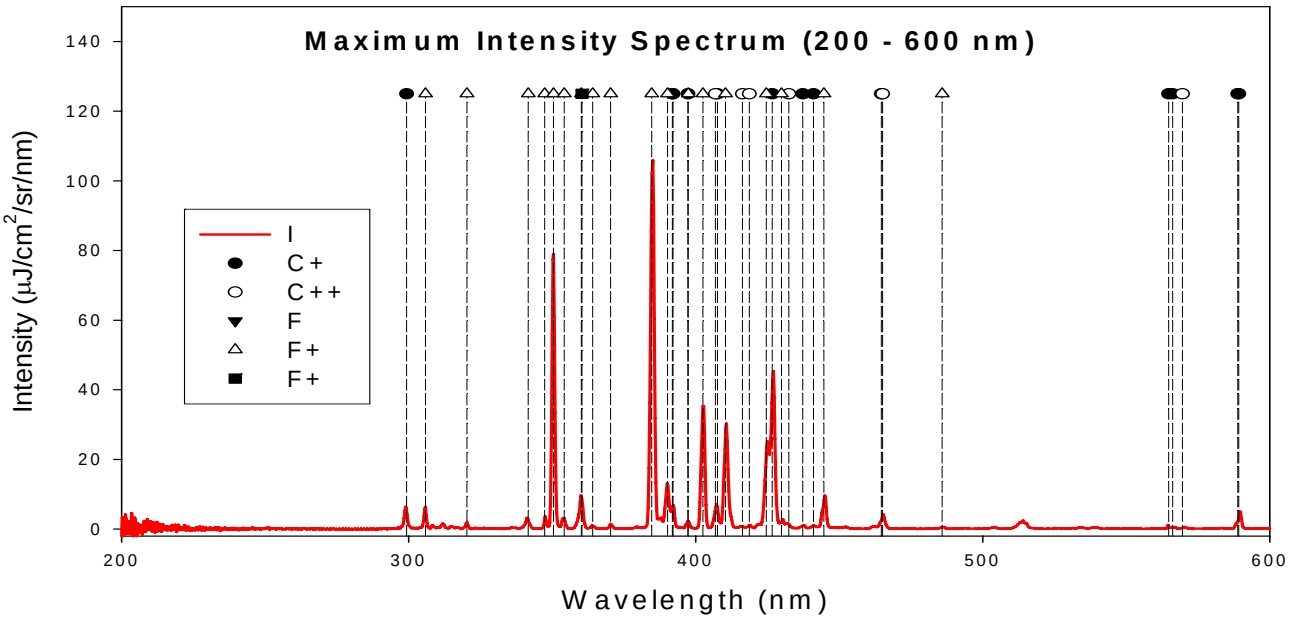

Figure 8. Spectrum at maximum intensity position 200 – 600 nm.

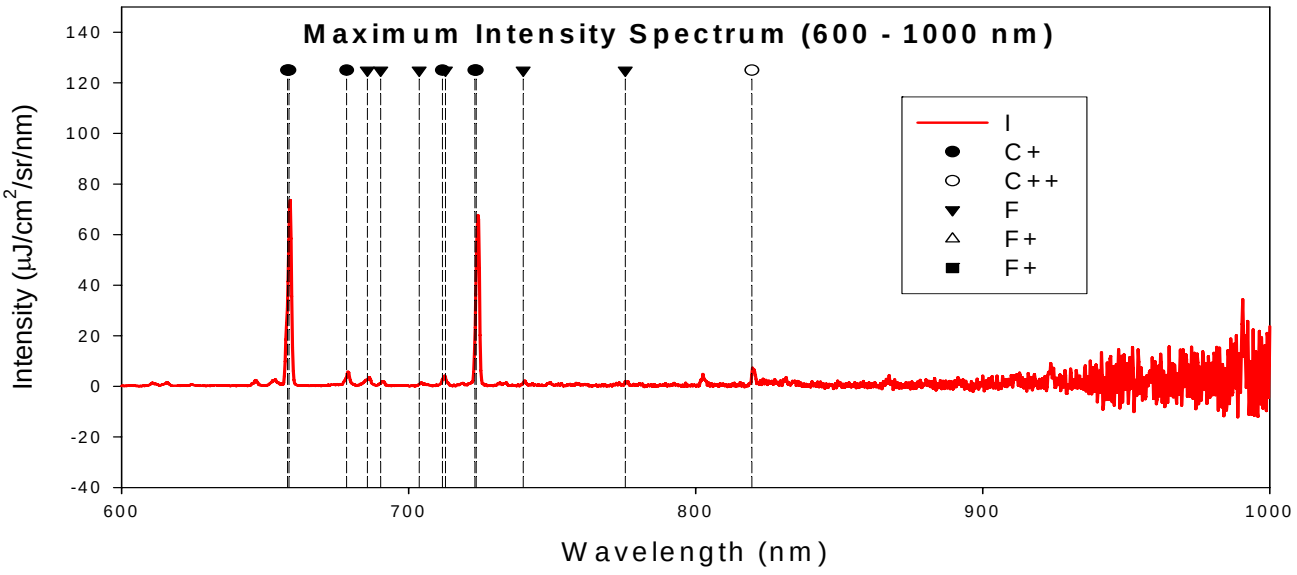

Figure 9. Spectrum at maximum intensity position 600 – 1000 nm.

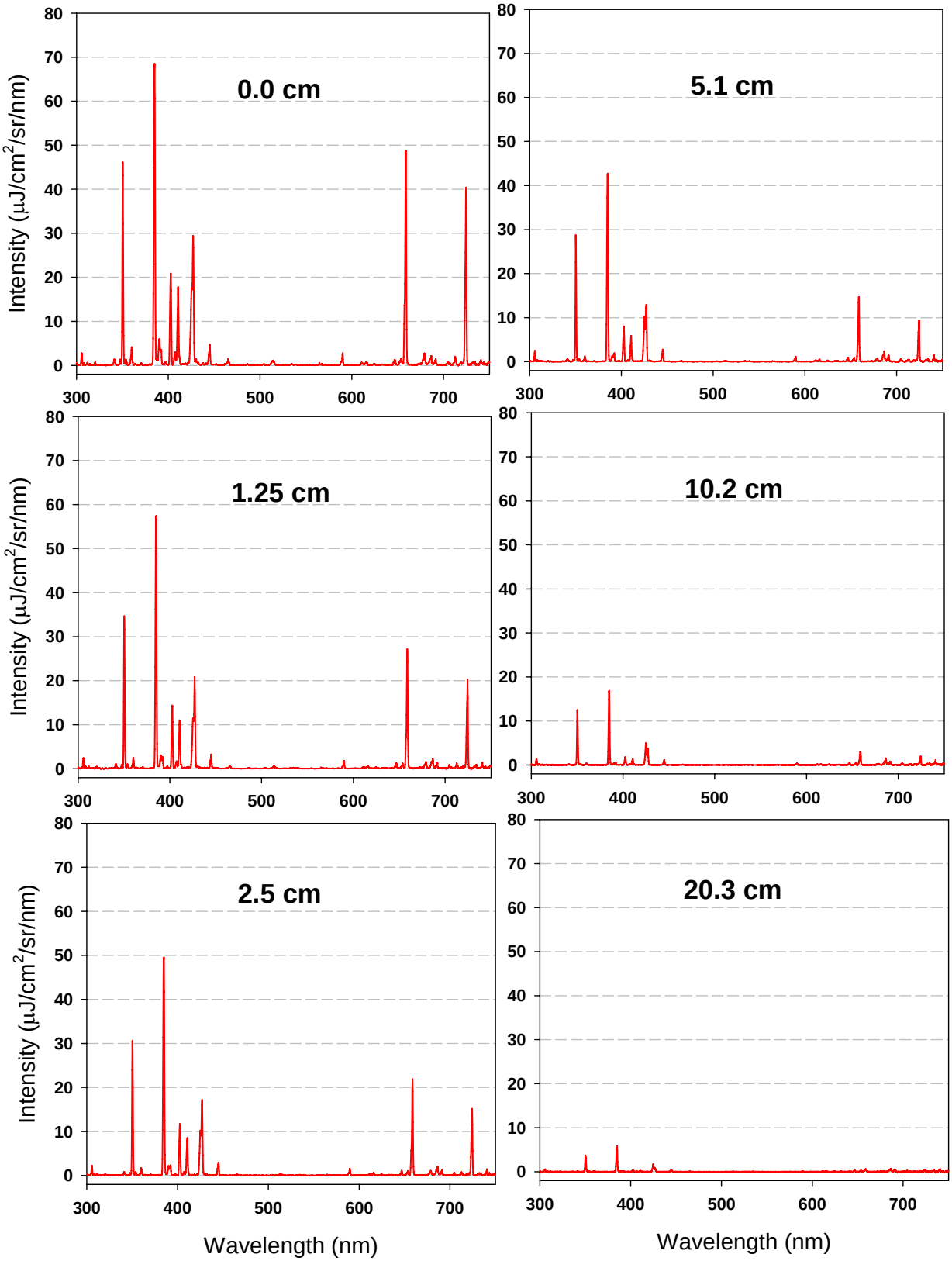

Figure 10. Spectra taken between 0.0 and 20.3 cm downstream of exit plane.

V. Extreme Ultraviolet Measurements

An instrument was built to measure the extreme ultraviolet radiation from a PPT. This instrument was a ten-barrel photometer that registered radiation from 1 to 200 nm from a pulsed source with low spectral resolution. It was designed to operate in vacuum and be resistant to electromagnetic interference (EMI). Each 15 inch (38 cm)-long, 1-inch diameter barrel was closed with two end-caps creating a sealed Faraday cage (see Figure 11). Two 3/8" (9.5 mm) diameter apertures separated by 13 inches (33 cm) assured that incoming radiation was collimated to approximately 3°. The front aperture was covered with a fine, electrically conductive mesh secured with conducting epoxy. The radiation exiting the second aperture passed through a spectral filter before striking a 1 cm x 1cm square detector.

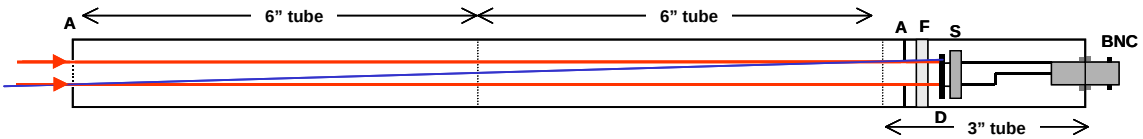

Figure 11. Scale drawing of a photometer barrel. The extreme off-axis ray (blue line) makes an angle of 1.6 degrees with the axis. Code: A = aperture; F = filter; D = detector; S = socket; BNC = BNC coax connector.

The ten barrels pass through a pair of round plates that constrain the barrels to aim to a common observation point. A motorized, non-conducting flag allows the radiation from the plasma source to be blocked without attenuating any high frequency EMI. The optical signal is the difference between the output pulse from the detectors with the flag down and the flag up. A photograph of the instrument mounted in the vacuum chamber next to the NIR-UV optic is shown in Fig. 12

Each output from the ten detectors was connected via a double-shielded cable and vacuum feedthrough to one of 10 channels of three digital sampling oscilloscopes (DSOs). A timing pulse from the PPT firing circuit triggered all ten channels of the DSOs simultaneously. The acquisition protocol was to record a 30 pulse average with the beam flag open (signal + noise) and a 30 pulse average with the beam flag blocking the entrance apertures of the photometers (noise). Subtracting the two averages yielded a signal that was proportional to the charge created by the photons registered in the detector.

That is, the voltage out of the detector is a time varying pulse $V(t) = R\, I(t)$, where R is the load resistance seen by the detector and $I(t)$ is the current through this resistance. The integrated area, A_V, under this voltage curve is proportional to the charge, $Q(t)$, released by the photon pulse, *viz.*,

$$A_V = \int V(t)dt = R\int \frac{dQ(t)}{dt}dt = \mathrm{e}\, N_e R = \mathrm{e}\, N_p R\, QE \qquad (1)$$

where e is the charge of an electron, N_e of electrons released by the photon pulse, and the quantum efficient is $QE = N_e/N_p$. Then the number of photons, N_p, per solid angle, $\Delta\Omega$, per area of plume viewed, ΔA_s can be written in terms of the time-integrated voltage (area of voltage pulse) registered on the DSO channel, A_V, as

$$\frac{N_p}{\Delta A \Delta\Omega} = \frac{A_V z^2}{\mathrm{e}\, \mathrm{R}\, QE\, A_s A_D}\,. \qquad (2)$$

Here A_D is the apertured area of the detector and z is the distance from the detector to the source.

All data were taken with the detectors unbiased and without amplification. Attempts to use amplification or biasing resulted in unacceptably high noise levels due to the approximately 3 m cable length between the detectors and electronics. A concern with using unbiased detectors is a possible nonlinearity relationship between the charge created by the photons and that registered by the electronics. An independent experiment proved that the detector output was linear for the entire dynamic range used.

The detector-filter combinations loaded in the 10-barrel photometer are given in Table 1 and the wavelength dependent response is presented in Figs. 13 and 14 for channels 2-10. Channel 1 employed an unfiltered UVG100[5] whose response varies significantly over the entire EUV NIR spectral interval (see inset in Fig. 16). For the purposes on estimating the photon flux impinging on this detector an average value of 0.62 was used in Eq. 2 for channel 1. This is obviously a significant approximation as the QE varies an order of magnitude over the 200-1000 nm spectral interval. Using an average QE for the other channels is not so severe an approximation. In Table 1 a

center wavelength was assigned for each detector to calculate a energy/photon (=hc/λ where h = 6.6 x 10^{-34} J-s and c = 3 x 10^{8} m/s and λ is the wavelength in meters) which is presented in the last column. These values are useful for estimating the energy flux from the photon flux (see Figures 16 and 17).

Figure 13 displays the quantum efficiency of the filtered detectors used in the photometer. Channels 2 – 7 used metal filters that were deposited direct-ly on detector surface. Channels 8-10 used UVG detectors[5] with Acton interference filters placed in front of them.[6] Note that the QE values shown for these last three detector-filter combina-tions are expanded 10X in Figure 13. No intensity standard was available for this spectral interval and all intensities presented rely on the QEs supplied by the detector manufacturer.

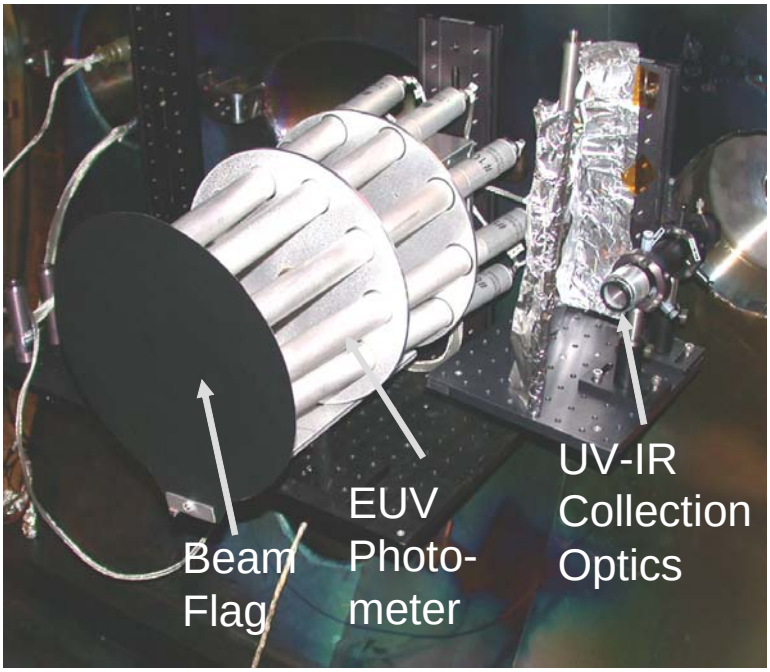

Figure 12. Photograph of the 10-barrel EUV photometer to the left of the IR-UV optical objective

Also shown in these figures are the spectral position and intensity of emissions lines from all ionizations degrees of carbon, and fluorine. These are for the experimentally observed emissions with relative intensities as listed by NIST.[7] The intensity levels are for a given species and are not to be applied between elements. Fluorine is expected to have twice the concentration of carbon.

Table 1
EUV Detector Parameters

Channel No.	Detector	WL Range (nm)	Avg QE	Median WL (nm)	E/photon (μJ)	Sensitivity*	Max Emsision*
1	UVG100	100-1000	0.62	450	4.4×10^{-13}	5×10^{12}	1.6×10^{14}
2	Al/Mn2	1.9 - 4	10	2	9.9×10^{-11}	3×10^{11}	--
3	Ti/C	< 7	10	4	5.0×10^{-11}	3×10^{11}	--
4	Zr/C	6 - 20	10	11	1.8×10^{-11}	3×10^{11}	--
5	Al4-1000	17 - 80	2	20	9.9×10^{-11}	2×10^{12}	4×10^{12}
6	In/SiC	76 - 99	3.8	90	2.2×10^{-12}	1×10^{12}	--
7	LA	117 - 131	0.6	125	1.6×10^{-12}	5×10^{12}	1.3×10^{13}
8	UVG/ACTON-138	130 - 150	0.0232	140	1.4×10^{-12}	1×10^{14}	2.7×10^{14}
9	UVG/ACTON-162	150 - 170	0.0700	160	1.2×10^{-12}	5×10^{13}	2.2×10^{14}
10	UVG/ACTON-178	170 - 190	0.0713	180	1.1×10^{-12}	5×10^{13}	-

*photons/pulse/cm^2/steradian

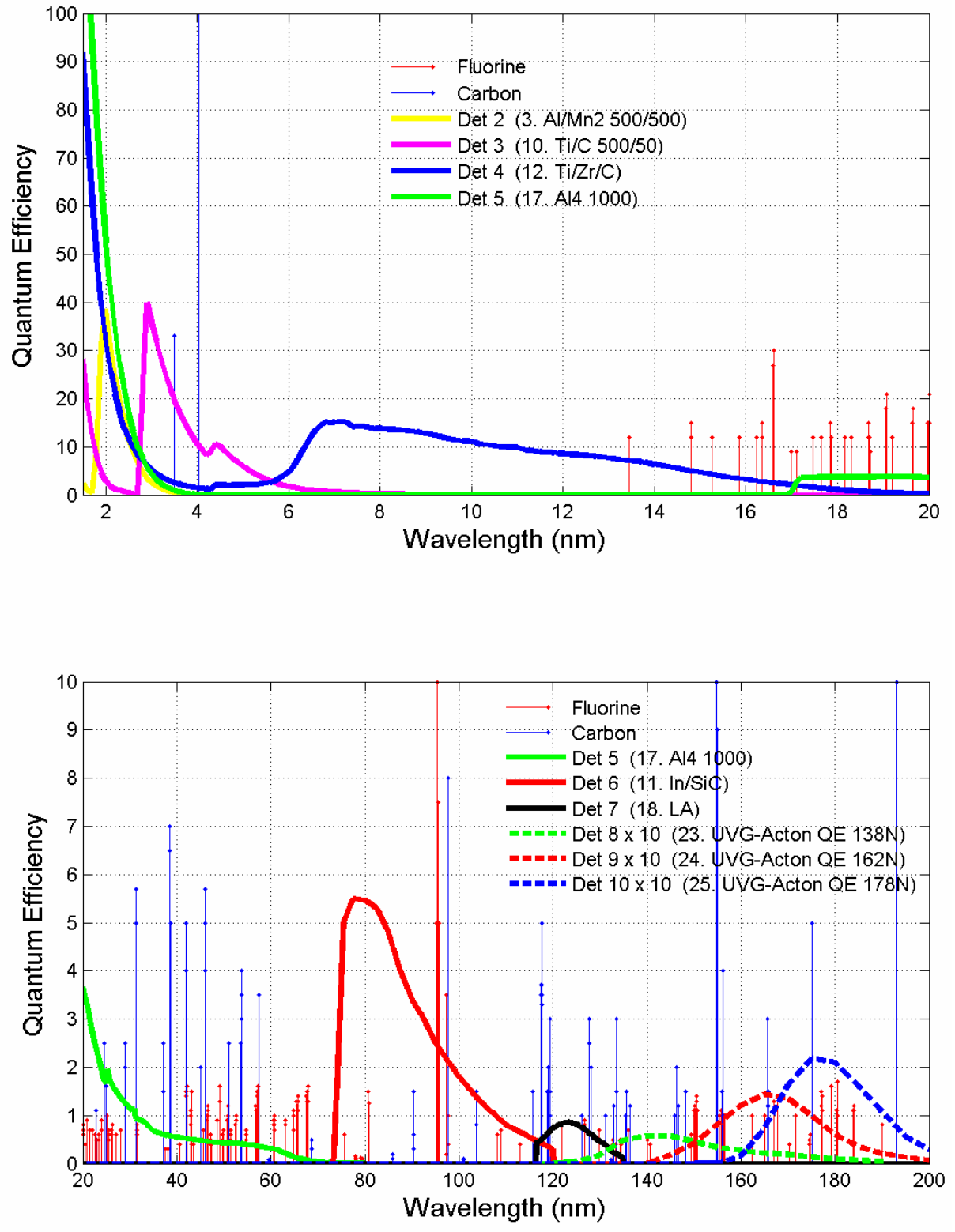

Figure 13. Quantum Efficiencies of channels 2 - 5 from 1 to 20 nm (above) and 5 – 10 from 20 to 200 nm (below). Note that the QE values of the channels 8-10 are magnified by a factor of 10. Spectral line positions and heights taken from NIST database.[7]

Measurements were taken in the plume at 33 positions downstream of the exit plane over a 30 cm range. The positions, every 25 mm along the centerline and 25 mm below the centerline, and every 50 mm along a line 50 mm below the plume centerline, are indicated in Figure 15. The field-of-field (FOV) of the instrument, also indicated in this figure, sampled circular cross section of approximately 25 mm diameter.

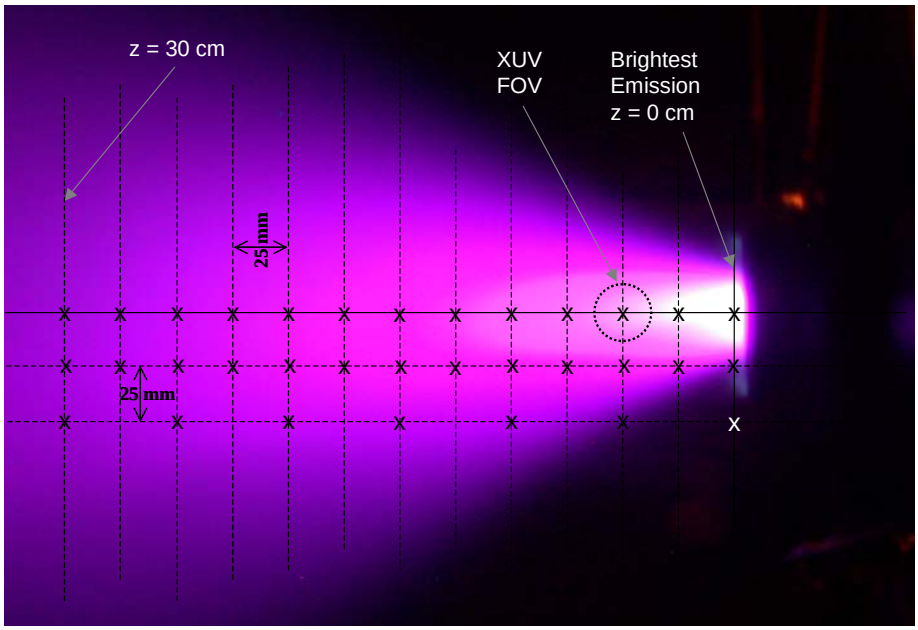

Figure 14. Positions of the XUV photometer measurements. The field-of-view is indicated as FOV.

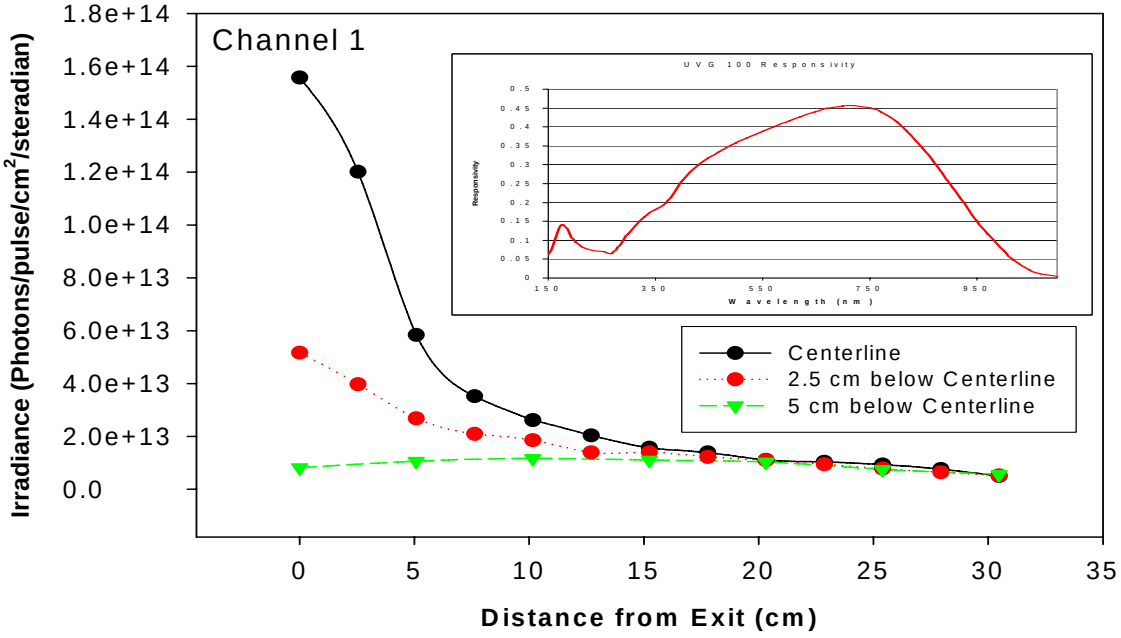

Figure 15. Emission from channel 1 of the XUV photometer. The inset shows the response of the unfiltered detector used in this channel.

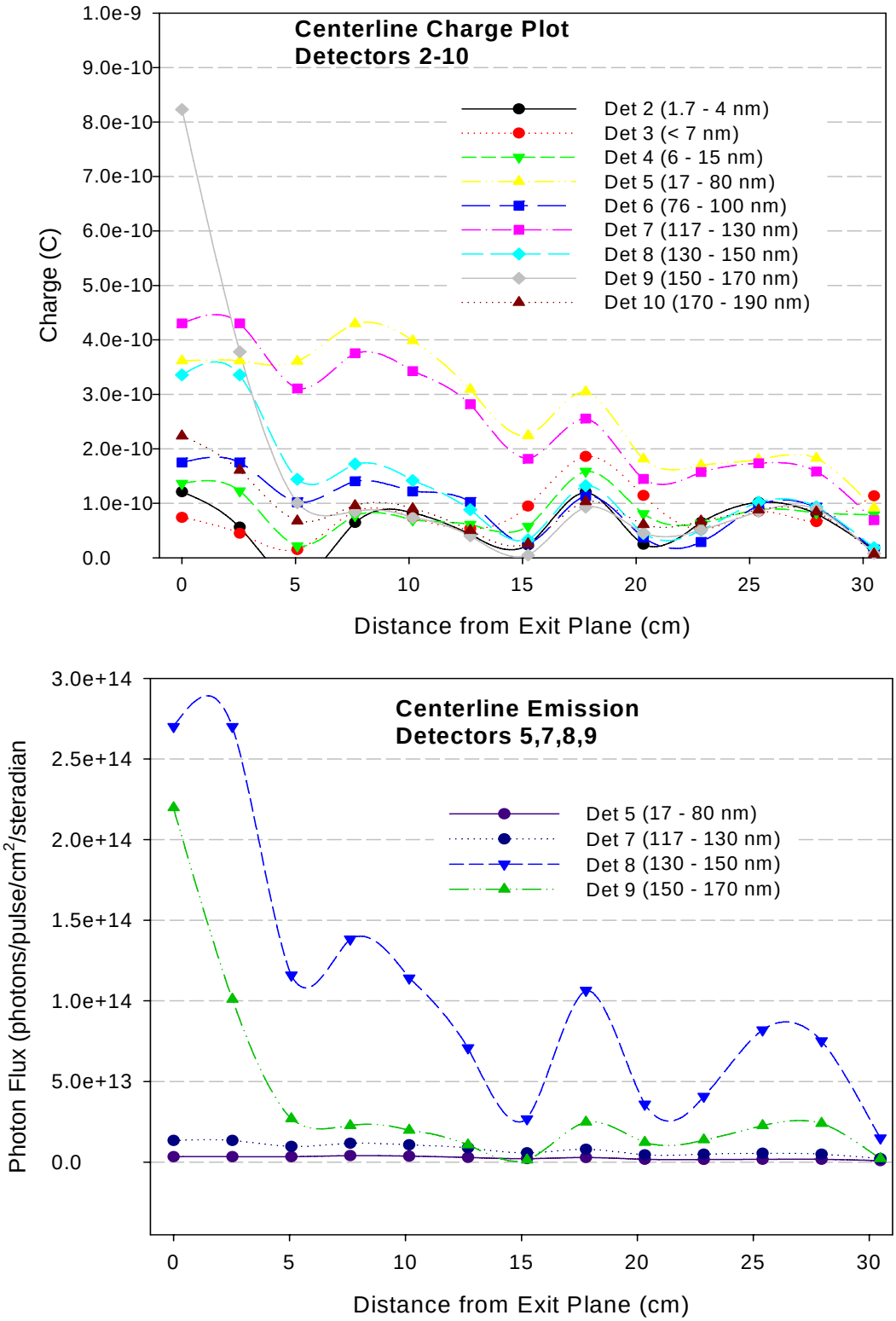

Figure 16. Centerline photon created charge in detectors 2-10 of the XUV photometer (upper panel) and approximate photon flux in the four channels registering emission (lower panel).

The photon flux measured from channel 1 is show in Figure 15. The smooth curves are indicative of a strong signal with very little noise component. Contrast this with the centerline signal from channels 2 – 10 shown in the upper panel of Figure 16. It is clear that the sensitivity of these channels is approximately 2 x 10^{-10} C. It is also clear that emission is seen above this level only in channels 5, 7, 8, and 9. Interestingly, the strongest emission in the 150-170 nm regions (Ch. 9) falls off most rapidly with distance from the exit plane. However, emission from the higher energy photons (Ch. 5 and Ch. 7) is more persistent. Emission from positions off the plume centerline is not discernable.

The charge shown in the upper panel of Figure 16 can be converted to photon flux for the four channels showing measurable emission using the quantum efficiencies given in Table 1. This result is shown in the lower panel of Figure 16. The data are presented as photon flux because the bandpass of each channel is wide. Median energies/photon are presented in Table 1 and these can be used to obtain a crude estimate of the energy flux per pulse. A more accurate estimate of the energy flux can be made by using the exact wavelengths of emissions.

With the aid of Figure 13, the origin of this emission can be discussed. It is speculated that the strong emission in the 150-170 nm regions (Detector 9) is likely due to strong carbon (CIV) lines near 155 nm. Although there are a number of fluorine lines under this transmission curve, most of these lines also fall within the passband of the 170-190 nm (Ch. 10) filter and there is no discernable emission in Ch 10. Furthermore, the emission in Ch. 8 has the same sharp decrease in intensity with distance from the exit plane as does Ch. 9 and the strong carbon (CIV) lines near 155 nm also falls under the Ch. 8 passband. Thus it is plausible that the emission registered in both channels 8 and 9 originate from the same group of C^{+3} lines.

Fig. 13 shows that the lines that fall within the passband of Ch. 7 (117-130 nm) are almost all from carbon. The decrease in this emission with distance from the PPT is slow compared to that in Ch. 9. This may be due to the fact that the carbon emissions in this spectral region are due to neutral carbon (CI), which will continue to emit at lower temperatures than triply ionized CIV seen in channels 8 and 9 if the temperature of the plasma decreases with distance from the PPT (see ionization potentials in Table 2). Measurements indicate that a PPT operating at discharge energy of 40 J/pulse have electron temperatures of 2 - 3 eV at 6 cm from the thruster exit, dropping to temperatures of 1- 2 eV at 20 cm from the exit.[10]

Table 2
Ionization Potentials (eV) [8, 9]

Ionization State	Fluorine	Carbon
I (Neutral)	17.4	11.26
II (1+)	35.0	24.4
III (2+)	62.65	47.9
IV (3+)	87.1	64.5
V (4+)	114	392
VI (5+)	157	490

The spatial emission profile of Ch. 5 (17-80 nm) is very similar to that of Ch. 7. Emission from species of both carbon and fluorine is seen in this passband. All the carbons lines of significant strength in this passband that are at wavelengths below 60 nm originate from CIII or higher ionization states of carbon. Fluorine has emission from both neutral (78–98 nm) and singly ionized species (61, 55, 51, 43-45, 31-37 nm) of significant intensities. These species of fluorine are more easily ionized than CIII suggesting that the emission registered in Ch. 5 may be from FII. However, the data are specific enough to identify the origin of this emission.

VI. Summary and Discussion

The goal of this study was to quantitatively measure the energy per pulse emitted from the Aerojet PPT from the mid infrared to the extreme ultraviolet (15 μm to 1 nm). This was accomplished using three instruments. In the mid infrared, a spectrograph with a helium cooled array detector measured emission from 2 μm to 13.5 μm; data from 6 - 8 μm were eliminated due to contamination by atmospheric water and instrument issues. A mid-range instrument measured 1 nm resolution absolute emission from 200 nm to 1000 nm. The third instrument, a 10-channel photometer, measured emission from 2 nm to 190 nm with low resolution.

In the mid IR the strongest emission feature at 4.42 μm had a maximum observed intensity of 9×10^{-7} μJ/pulse/cm^2/sr/μm at the exit plane. The IR emission did not decrease monotonically with the distance from the thruster as the emission at 100 cm from the exit plane was generally greater than that at the 50 cm position. This indicates that the populations of the excited states emitting this radiation are increasing most likely by cascade from higher levels. Assuming that the velocity of the streaming plasma is 15 km/s[4], this process is occurring on the time scale of 50 – 100 μs. Emission by this instrument could be observed to wavelengths beyond 10 μm.

The mid-range instrument registered rich discrete spectra showing at least 75 features, 51 of which can be assigned to F, F^+, C^+, and C^{++}. A band attributed to C_2 could also be discerned near 515 nm. These results are consistent with the spectra recorded by Markusic and Spores[4] who studied the temporal characteristics of the emission in the 350-750 nm spectral interval for a PPT operated at discharge energies of 15 J, 25 J, and 45 J. They found that increasing the discharge energy does not appreciably alter the relative intensity of the lines in the spectra indicating that the plasma temperature (measured to be near 1.4 eV or 16,000K) is independent of the discharge energy. The greatest spectral intensity observed here was 100 μJ/pulse/cm^2/sr/nm (= 10^5 μJ/pulse/cm^2/sr/μm) for the F^+ line near 390 nm. This radiation decreased monotonically with increasing distance from the thruster exit plane to 20 cm, the maximum distance with observable emission for this instrument's sensitivity.

The 10-channel XUV photometer registered emission in 5 channels. The broadband channel showed a steep decreased in emission in the first 10 cm from the exit plane. The 17 – 80 nm and the 117 – 130 nm channels showed measurable emission to 20 cm beyond the exit whereas the 130 – 15 nm and the 150 – 170 nm channels dropped to background intensity in the first 5 cm. The 17 – 80 nm emission is may be due to F^+ and the emission from the 130 – 150 nm and 150 – 170 nm channels is attributed to C^{+++}. The emission from the 117 – 130 nm channel is consistent with that originating neutral carbon (C). The maximum emission was seen in the 130 – 150 nm channel. Assuming that the wavelength of this emission is 140 nm, the energy flux is 350 μJ/pulse/cm^2/sr.

The total energy emitted by the PPT is obtained by first integrating the spectral flux over the profiles of individual features to obtain the energy/pulse/cm^2/sr. The resulting flux must be integrated over the area using the profiles measured here to build a model of the spatial dependence of the emission. To perform the integration over the solid angle, one must appeal to a theoretical model for the (unmeasured) angular dependence. Performing these integrations over all features will produce the total energy emitted per pulse throughout the observed spectral extent of the instrument.

It is instructive to compare the spectral energy flux measured by the broadband detector in the photometer with that of the flux seen in the highest emitting line measured by the mid-range instrument. The Doppler width [$\Delta\lambda/\lambda = 3.6 \times 10^{-7} \times (T/amu)^{1/2}$] of the F^+ line at 390 nm at a temperature of 16,000 K is 4×10^{-3} nm. The flux from this line is (100 μJ/pulse/cm^2/sr/nm) x (4×10^{-3} nm) = 0.4 μJ/pulse/cm^2/sr. From Table 1 and Figure 16 the integrated flux from < 200 nm to 1.1 μm is (1.6×10^{14} photons/pulse/cm^2/sr) x (4.4×10^{-13} μJ/photon) = 70 μJ/pulse/cm^2/sr/nm. Although the approximations in the quantum efficiency and possibly the linewidth are considerable, this calculation does illustrate that this strongest line carries on the order of a percent of the radiation seen over this wide spectral interval.

In conclusion, the magnitude and wavelength of emissions observed are compatible with imaging satellite applications provided PPTs are placed appropriately relative to the fields-of-view of on-board instruments.

Acknowledgments

The authors thank Daryl L. Kim and Richard J. Rudy for assistance in acquiring and analyzing data from the BASS instrument. Nicole Meckel of Aerojet provided engineering support for the PPT throughout this work. This work was partially supported by The Aerospace Corporation's Independent Research and Development Program.

References

[1]Hoskins, W. A., Wilson, M. J., Meckel, N. J., Campbell, M., Chung, S., "PPT development efforts at Primex Aerospace Corporation," AIAA-99-2291, *35th AIAA/ASME/SAE/ASEE Joint Propulsion Conference & Exhibit*, Los Angeles, California, 20-24 June 1999.

[2]Garrett, M. G., Beiting, E. J., Caven, W., Cory, R., "Electromagnetic Emissions from DC to 17 GHz from a Pulsed Plasma Thruster (PPT)," International Electric Propulsion Conference, IEPC 2007-269, Florence, Italy, 2007

[3]J. A. Hackwell, D. W. Warren, M. A. Charclain, Y. Dotan, P. H. Li, D. K. Lynch, D. J. Mabry, R. W. Russell, and R. M. Young. "A Low Resolution Array Spectrograph for the 2.9 to 13.5 Spectral Region," SPIE Vol. 1235 Instru. In Astronomy VII (1990).

[4]Markusic, T. E. and Spores, R. A. "Spectroscopic emission Measurements of a Pulsed Plasma Thruster," 33rd AIAA/ASME/SAE/ASEE Joint Propulsion Conf. and Exhibit, AIAA-1997-2924, Seattle, WA, July 6-9, 1997.

[5]International Radiation Detectors (IRD), Torrance CA.

[6]Acton research Corporation, Acton MA.

[7]http://physics.nist.gov/PhysRefData/ASD/index.html (spectral lines)

[8]http://physics.nist.gov/PhysRefData/IonEnergy/tblNew.html (ionization potentials)

[9]Weast, R. C. ,ed. CRC Handbook of Physics and Chemistry, 49th Edition, The Chemical Rubber Co. Cleveland, OH, 1968.

[10]Gatsonis, N. A., Eckman, R., Yin, X., Pencil, E .J., Myers, R. M., "Experimental Investigations and Numerical Modeling of Pulsed Plasma Thruster Plumes," *J. Spacecraft Rockets*, 38, 454-464 (2001).